4-16-2018

Electrical and material properties of hydrothermally grown single crystal (111) UO2

Christina L. Dugan
Air Force Institute of Technology, Christina.Dugan@afit.edu

George Glenn Peterson
University of Nebraska - Lincoln

Alyssa Mock
University of Nebraska - Lincoln, alyssalynnmock@gmail.com

Christopher Young
Air Force Institute of Technology

J. Matthew Mann
Wright-Patterson Air Force Base

See next page for additional authors

Dugan, Christina L.; Peterson, George Glenn; Mock, Alyssa; Young, Christopher; Mann, J. Matthew; Nastasi, Michael; Schubert, Mathias; Wang, Lu; Mei, Wai-Ning; Tanabe, Iori; Dowben, Peter A.; and Petrosky, James, "Electrical and material properties of hydrothermally grown single crystal (111) UO2" (2018). *Faculty Publications from the Department of Electrical and Computer Engineering*. 516.
https://digitalcommons.unl.edu/electricalengineeringfacpub/516

Authors

Christina L. Dugan, George Glenn Peterson, Alyssa Mock, Christopher Young, J. Matthew Mann, Michael Nastasi, Mathias Schubert, Lu Wang, Wai-Ning Mei, Iori Tanabe, Peter A. Dowben, and James Petrosky

THE EUROPEAN
PHYSICAL JOURNAL B

Regular Article

Electrical and material properties of hydrothermally grown single crystal (111) UO$_2$

Christina L. Dugan[1,a], George Glenn Peterson[2], Alyssa Mock[3], Christopher Young[1], J. Matthew Mann[4], Michael Nastasi[1,5], Mathias Schubert[3], Lu Wang[6,7], Wai-Ning Mei[7], Iori Tanabe[6], Peter A. Dowben[8], and James Petrosky[1]

[1] Department of Engineering Physics, Air Force Institute of Technology, 2950 Hobson Way, Wright-Patterson Air Force Base, OH 45433-7765, USA
[2] University of Nebraska, Walter Scott Engineering Center, Lincoln, NE 68588-0656, USA
[3] Department of Electrical and Computer Engineering, University of Nebraska, Walter Scott Engineering Center, Lincoln, NE 68588-0511, USA
[4] Air Force Research Laboratory, Wright-Patterson Air Force Base, OH 45433-7765, USA
[5] Nebraska Center for Energy Sciences Research, University of Nebraska, 230 Whittier Research Center, 2200 Vine Street, Lincoln, NE 68583-0857, USA
[6] CAS Key Lab of Materials for Energy Conversion, Department of Materials Science and Engineering, University of Science and Technology of China, Hefei, Anhui 230026, P.R. China
[7] Department of Physics, University of Nebraska at Omaha, 60th and Dodge Streets, Omaha, NE 68182-0266, USA
[8] Department of Physics and Astronomy, University of Nebraska-Lincoln, Theodore Jorgensen Hall, 855 North 16th Street, Lincoln, NE 68588-0299, USA

Abstract. The semiconductor and optical properties of UO$_2$ are investigated. The very long drift carrier lifetimes, obtained from current–voltage $I(V)$ and capacitance–voltage $C(V)$ measurements, along with the well-defined optical properties provide little evidence of an abundance of material defects away from the surface region. Schottky barrier formation may be possible, but very much dependent on the choice of contact and surface stoichiometry and we find that Ohmic contacts are in fact favored. Depth resolved photoemission provided evidence of a chemical shift at the surface. Density functional theory, with the Heyd-Scuseria-Ernzerhof (HSE) functional, indicates a band gap of a 2.19 eV and an anti-ferromagnetic ground state. Ellipsometry measurements indicates at UO$_2$ is relatively isotropic with a band gap of approximately 2.0 eV band gap, consistent with theoretical expectations.

1 Introduction

The rapid depletion of ^{3}He resources, and the desire for vibration insensitive, radiation hard devices dominates the search for alternative neutron detector technologies [1], used for tracking fissile materials. The ultimate goal is an efficient, compact, low power detector relatively unaffected by terrestrial temperature changes. As an example, icosahedral semiconducting boron carbides [2–6] have recently garnered interest because they meet many of the operational requirements, but they still need significant neutron moderation to be efficient in detecting neutrons from fissile materials.

A novel approach explored in this research is a solid state neutron detector composed of UO$_2$. Uranium has the unique (among semiconductors) feature of a high fission cross section, making it a valuable medium for detection because of the potential for very large signal to noise generation. It has been studied as a neutron absorber

since the 1930s [7]. In recent years, although somewhat limited, there have been efforts to explore the geometric and electronic properties of UO$_2$ for the purpose of semiconductor device fabrication [8–10]. Primarily focused on the prospects of neutron detection and photovoltaics, the concept has been largely undeveloped due to the difficulty for material growth [8,10] Single crystal growth of actinides for application to electronics is complex due to the very large electron–phonon coupling, lattice deformations, and significant changes in Debye temperature, mediated through Jahn-Teller distortions [11]. These latter effects are unusual, as UO$_2$ is a true semiconductor, not a metal, so phonons cannot couple to the Fermi Sea of electrons or holes.

Given the orthorhombic allotrope of α-phase uranium metal, the fluorite structure of UO$_2$, and the rapid oxidation and large range of O/U ratios, it is difficult to control sample stoichiometry without strictly controlling temperature and pressure of the growth environment [12]. A further complication exists: while defect creation is expected to occur at high(er) temperatures, especially

^{a} e-mail: Christina.Dugan@afit.edu

above 1000 K; the simplified phase diagram of the UO_x system suggests a UO_{2+x} to UO_{2+x} and U_4O_{9-y} transition between 473 and 670 K [13,14]. Such a structural phase transition would alter the density of lattice imperfections and a change in defect density would enhance Jahn-Teller distortions significantly [11,15].

The challenges of growing high-quality uranium oxide single-crystal have begun to be addressed with the fabrication of high-quality, single crystal actinide oxide samples using a hydrothermal synthesis growth technique [16]. This growth process has produced bulk single crystals of near-stoichiometric UO_2. These improved single crystals open the door to a much better assessment of the optical and semiconductor properties, not previously possible.

2 Experimental

Single crystals of UO_2 were grown by hydrothermal synthesis using a nutrient/feedstock of high-purity, depleted uranium dioxide powder (99.998% UO_2, International Bioanalytical Laboratories, Lot# B206093). A 6M cesium fluoride mineralizer solution (99.9% CsF, Alfa Aesar, Lot# S25A038) was utilized to aid dissolution of the nutrient and transport it to the colder crystallization zone of the reaction vessel. The temperature of the feedstock and crystallization zones were held at 650 °C and 600 °C, respectively for 45 days at a pressure of 25 kpsi. The feedstock, mineralizer and seed crystals were loaded into an inert sealed silver ampule (99.95% Ag, Refining Systems, Inc.) and then welded shut. CaF_2 seeds with (111) orientation provided a template for oriented growth of 0.10 mm UO_2 on the substrate. Orientation and crystal structure was confirmed by single-crystal X-ray diffraction. UO_2 crystals grown under these conditions have measured lattice parameters of 5.4703 ± 0.0006 Å indicating a stoichiometry near $UO_{2.003}$ [13,17]. The resultant (111) UO_2 crystal's triangular surface area measured approximately 21 mm².

Contacts on a triangular 21 mm² (111) UO_2 sample were fabricated at 20 °C using a paint/melt deposition technique as well as mechanical placement. The circular Ag paint contact with radius of approximately 2.9 mm, was fabricated by application of Ag (Delco Conductive Ag Paint, #16062). The opposing circular GaIn paint/melt contact with radius of approximately 4.5 mm was fabricated by applying a GaIn eutectic (Aldrich Gallium-Indium eutectic, >99.99% trace metals) to the UO_2 (111) sample. Mechanical contacts were made by pressing sharpened tungsten pins into opposing facets of the crystal. Micron thick Cu wires were then affixed to the contacts allowing current–voltage, $I(V)$, and capacitance–voltage, $C(V)$, measurements using a semiconductor analyzer system. The paint/melt two-point circuit used the Ag contact as the positive voltage reference. The work function of polycrystalline Ag is 4.26 eV, slightly higher than that of GaIn, 4.1–4.2 eV making possible Ohmic contact surfaces [18,19].

The variable angle spectroscopic ellipsometry (VASE) data was obtained using a dual-rotating compensator ellipsometer (RC2, J.A. Woollam Co., Inc.), using a
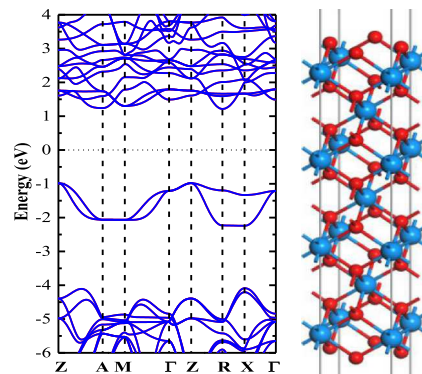
Fig. 1. The band structure of bulk UO_2 (schematically shown with O: red; U: blue) using Heyd-Scuseria-Ernzerhof (HSE) hybrid functional. The band gap is 2.19 eV and the ground state is anti-ferromagnetic.

wavelength-by-wavelength approach. The 0.1 mm UO_2 layer atop the 1 mm CaF_2 substrate was assumed to be bulk and therefore, the CaF_2 layer was neglected. This method allowed for the determination of the dielectric response of the bulk top layer UO_2. Measurements were taken at angles of incidence 45°, 55°, 65°, and 75° from 0.7 to 6.4 eV. The sample was modeled using a simple two phase (ambient-substrate) approach where the substrate represents single-crystal UO_2, ignoring surface overlayer effects. Data was analyzed using WVASE32 (J.A. Woollam Co., Inc.).

3 Theory

All density functional theory calculations were performed within the framework of spin-polarized plane-wave density functional theory (PW-DFT), as implemented in the Vienna ab initio simulation package (VASP) [20]. The generalized gradient approximation (GGA) with the Perdew-Burke-Ernzerhof (PBE) functional and projector augmented wave (PAW) potentials were used for geometry optimizations [21–24], and specifically the exchange correlation was treated with the Perdew-Burke-Ernzerhof (PBE) functional [23]. In addition, to correct the strong on-site electronic correlation, the DFT+U method was used for the U atoms with $U - J = 4$ eV. We used the simplified approach to the DFT+U introduced by Dudarev et al., where only the difference $(U - J)$ is used to describe the electron correlation from different orbital momentum, U and J are the spherically averaged matrix elements of the screened Coulomb interaction [25].

We constructed the slab model for the UO_2 (111) surface with seven U atomic layers and eight O atomic layers, as shown in Figure 1. A vacuum layer, thicker than 15 Å between two adjacent slabs, was inserted in order to make the interactions between the slabs negligible. Geometrical structures were relaxed until the force on each atom was less than 0.01 eV/Å and the energy convergence criteria of $<10^{-7}$ eV was met. The 2D Brillouin zone integration using the Monkhorst-Pack Γ-center scheme was sampled with a $9 \times 9 \times 1$ grid [26]. The Bader's atom in molecule

(AIM) method based on the calculated charge density used for charge population analysis [27].

The Heyd-Scuseria-Ernzerhof (HSE) hybrid functional was also used to confirm the PBE+U results and we noticed that the new approach was more efficient in reaching convergence [28]. To complement density functional theory computation, the Cambridge Serial Total Energy Package (CASTEP) code was also adopted [29].

4 Results and discussion

The $I(V)$ measurement was used to evaluate the electrical contacts of the metal-semiconductor interfaces [18]. Knowing the work function of the metals (φ_M) and the electron affinity (χ) allows for the prediction of the barrier height (φ_B) if a Schottky (metal-semiconductor) diode has been formed from equations (1) and (2), where E_g is the semiconductor band gap [30].

$$\varphi_B = \varphi_M - \chi \quad \text{if the semiconductor is n-type,} \quad (1)$$

$$\varphi_B = E_g + \chi - \varphi_M \quad \text{if the semiconductor is p-type.} \quad (2)$$

The fluid metal eutectic, Ga-In or "EGaIn" forms an Ohmic contact with thin-films devices due to its tendency to make low contact-resistance structures and has been chosen as the anode contact material [19]. The polycrystalline colloidal silver paste contact was deposited by vacuum evaporation.

The band gap E_g for UO_2 has been established as $2.1 \pm 0.1\,\text{eV}$ [31]. In the flat band approximation, χ is the determined by subtracting band gap E_g from the photoemission work function. The photoelectric work function of the (111) hydrothermally grown UO_2 was measured at $6.28 \pm 0.36\,\text{eV}$ providing an electron affinity of $4.2\,\text{eV}$ [11]. Making use of equations (1) and (2) for the (111) UO_2, if the semiconductor is n-type, $q\phi_{\text{Bn0}} = 0.56\,\text{eV}$. If the semiconductor is p-type, the barrier $q\phi_{\text{Bp0}}$, is $1.5\,\text{eV}$.

The band gap is vastly under estimated in density functional theory, under the Perdew-Burke-Ernzerhof (PBE) functional, even with a correlation energy "turned on", i.e. $E_g = 0.28\,\text{eV}$. For CASTEP with PBE+U with a correlation energy of $U = 4\,\text{eV}$ applied to the f-states and the ultrasoft pseudopotential, the band gap is only slightly better $\sim 0.56\,\text{eV}$, based on different convergence schemes. However, with the Heyd-Scuseria-Ernzerhof (HSE) hybrid functional, the band gap comes out more correctly; but it is nonetheless clear that the $5f$ levels are very much a part of the band structure.

For VASP with PBE+U and plane augmented wave (PAW) pseudopotential: the UO_2 ground state is antiferromagnetic as is also indicated by VASP calculations undertaken with the HSE hybrid functional. For CASTEP with PBE+U and the ultrasoft pseudopotential, UO_2 is ferromagnetic while it is ferrimagnetic in the slab calculation using the HSE hybrid functional. The convergence process of VASP was quite smooth.

Experimentally, the electron affinity, χ is the determined by subtracting the calculated band gap E_g from the highest occupied molecular orbital energy state (HOMO). Photoemission spectroscopy (PES) measurements with
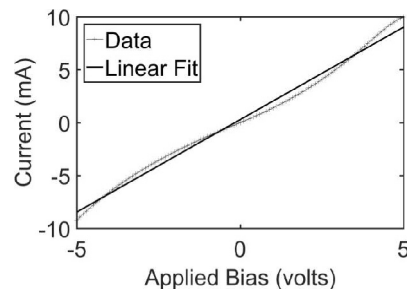

Fig. 2. The current versus voltage measurements of $Ag/UO_2/E$-GaIn metal-semiconductor Schottky device. The nearly linear data indicates a minimal barrier to charge carriers but is inconclusive as to the semiconductor majority carrier.

the established E_g indicate an electron affinity of $4.18\,\text{eV}$ for the (111) crystal orientation. Making use of equations (1) and (2), if the semiconductor is n-type, $\varphi_{\text{Bn0}} = 0.56\,\text{eV}$. If the semiconductor is p-type, $\varphi_{\text{Bp0}} = 1.5\,\text{eV}$. The near linear $I(V)$ response of Figure 2 clearly shows behavior near Ohmic behavior, i.e. a very small barrier to charge carriers. The energy of the Schottky diode is reduced by holes flowing from the metal to the semiconductor hence causing accumulation near the junction. Such a device is dominated by the electron flow from the semiconductor to the metal with essentially no recombination in the depletion region. Since the behavior is Ohmic there are two options for majority carriers at the junction. A p-type semiconductor metal interface can respond Ohmically, since the work function of UO_2 is close to or larger than the sum of the electron affinity and the band gap energy. However, if the semiconductor is strongly n-type, then current flow could appear Ohmic due to tunneling. Therefore, the $I(V)$ plot is inconclusive as to majority carrier.

Although the reverse bias behavior of a Schottky diode mimics that of a p–n junction (allowing for the $1/C^2$ determination of V_{bi} by linear extrapolation), the forward bias a.c. response is fundamentally different, since it is a majority carrier device. There is negligible diffusion current, and therefore negligible minority carrier charge injection and storage within the semiconductor. Instead stored carriers result in diffusion admittance. In the absence of stored carriers, there is no diffusion capacitance or diffusion conductance. As a result, at frequencies routinely approaching the GHz range, the device capacitance and conductance remain frequency independent. However, this is not what is observed in the data of Figure 3. The measurement of capacitance versus frequency ($C(f)$), and conductance versus frequency ($G(f)$) clearly show a frequency dependent response, with charge carriers that no longer respond at $10\,\text{kHz}$. This departure from the ideal is an indication of defects within the semiconductor.

Figure 4 shows the capacitance versus voltage curves for different perturbation frequencies. Again, the frequency dependence in reverse bias is evident as the capacitance is reduced with increasing perturbation frequency. A $1/C^2$ extrapolation has been performed to determine φ_B, and is shown as an inset in Figure 4. The effective barrier height was found to be $\varphi_B = 1.28\,\text{eV}$. Although not completely
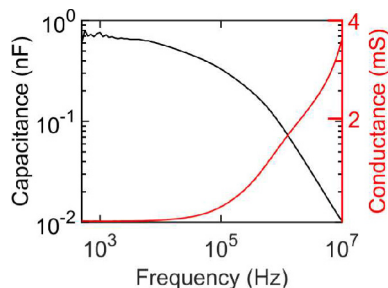
Fig. 3. The capacitance versus frequency and conductance versus frequency (semi-Log scale) measurements of Ag/UO$_2$/E-GaIn MS Schottky device. The frequency dependence of the data beginning at 10 kHz shows the presence of defects within the device.

Fig. 4. The capacitance versus voltage measurement for the perturbation frequencies 100 kHz, 1 MHz, and 10 MHz. The inset is a $1/C^2$ extrapolation for the determination of the effective barrier height $\varphi_B = 1.28$ eV.

equivalent, this barrier height coincides closer with the $I(V)$ barrier height for p-type UO$_2$ from our previous calculations.

While Figure 3 indicates the presence of defects, it is unclear as to their location (bulk or interface). However, the frequency at which the capacitance begins to increase provides evidence of defect type. For example, it has been shown in Si p–n homojunctions that defects due to vacancies and interstitial oxygen complexes cannot respond to oscillations near the 10^4 Hz range [32], whereas other defects do. The $C(V)$ curves, at 100 kHz and 1 MHz frequencies of the UO$_2$ Schottky diode are plotted in Figure 5. Ignoring defects and various contributions to capacitance, the drift carrier lifetime can be modeled by comparing the measured $C(V)$ curve and the modeled diffusion capacitance in the region of small forward bias. The frequency dependent diffusion capacitance, C_D, is given by:

$$C_D = \frac{G_0}{\omega\sqrt{2}} \left(\sqrt{1 + \omega^2\tau^2} - 1 \right)^{1/2}, \qquad (3)$$

where ω is the angular frequency ($2\pi f$), and τ is the drift carrier or effective carrier lifetime. The low frequency conductance, G_0, is calculated from the dc $I(V)$ values by numerical differentiation. Utilizing G_0 and f from the experiment, τ can be iteratively adjusted to ensure the C_D curve fits the $C(V)$ data. The lifetime, τ, controls the height and the slope of the modeled C_D to the measured $C(V)$ data and yields a drift carrier lifetime. Using this method, the Ag/UO$_2$ Schottky diode at 100 kHz is found to have a drift carrier lifetime ranging from 50 μs to 250 μs suggesting while defects are present, they are either not trap or scattering defects, or relatively few in number.

To ascertain whether the surface defects differ from the bulk, depth resolved X-ray photoemission spectroscopy (XPS) measurements of the U $4f$ region of the (111) UO$_2$ sample surface were taken using Al Kα radiation prior to contact placement. The XPS showed indications of higher surface oxidation states of uranium. The binding energy of both doublet peaks increase from the expected energies of U^{+4} at 0°, the condition in which the electron analyzer is normal to the sample surface, to higher binding energies at steep angles, indicating a chemical shift at the
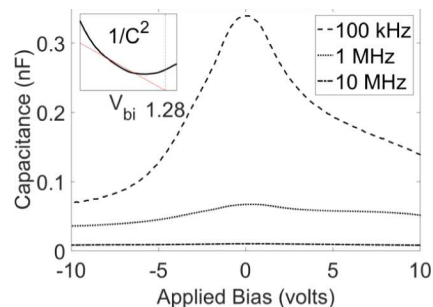
surface. The maximum sampled depth is estimated to be 50 Å at 0° based on the attenuation of an 1100 eV photoelectron [11]. Surface sensitivity is enhanced by altering the orientation angle of the electron analyzer away from 0°, normal to the surface, with an information depth of approximately 40 Å (Fig. 6).

We estimate the depth of the p-type surface layer to be less than 40 Å based on the depth-resolved XPS measurement. Willis [33] showed that a hyper-stoichiometric (effectively p-type) UO$_{2+x}$ in the cubic fluorite structure is possible by the incorporation of interstitial oxygen. Willis concluded that the defect complex is comprised of 2 anion vacancies, 2 $\langle 111 \rangle$ interstitial oxygen atoms, and 2 $\langle 110 \rangle$ interstitial oxygen atoms. The $C(f)$, $G(f)$, and photoemission data all support the presence of a hyper-stoichiometric layer at the surface of the UO$_2$ crystal. Analysis shows that this layer is approximately 40 Å deep. Due to the presence of defects at the surface, and the low number of charge carriers of the bulk semiconductor material, near the surface, the material is effectively p-type creating a metal-semiconductor Schottky barrier with the Ag metal contact. The extremely narrow range of this region explains the discrepancy between the predicted barrier height of this contact of 2.08 eV and the effective barrier of 1.28 eV from the C(V) data. Fowler-Nordheim tunneling is known to dominate in devices as wide as 1200 Å [34], although our data presently cannot support this. Overall, it seems that the material, unusual for an oxide, is p-type [35].

Variable angle spectroscopic ellipsometry (VASE) measurements, made at several azimuthal orientations, tends to verify that the sample is isotropic. This is important as some have concluded there is uniaxial anisotropy [36]. There was no significant evidence of anisotropy in the variable angle spectroscopic ellipsometry (VASE) data. Spectroscopic ellipsometry is an indirect measurement technique, which utilizes changes in polarization of light reflected off or transmitted through a sample [37,38]. An appropriate physical model is necessary to accurately describe the optical properties of the material. Values of the complex dielectric function of an unknown material can be found by a wavelength-by-wavelength regression analysis. Electronic band-to-band transitions cause critical point (CP) features in the dielectric function spectra.
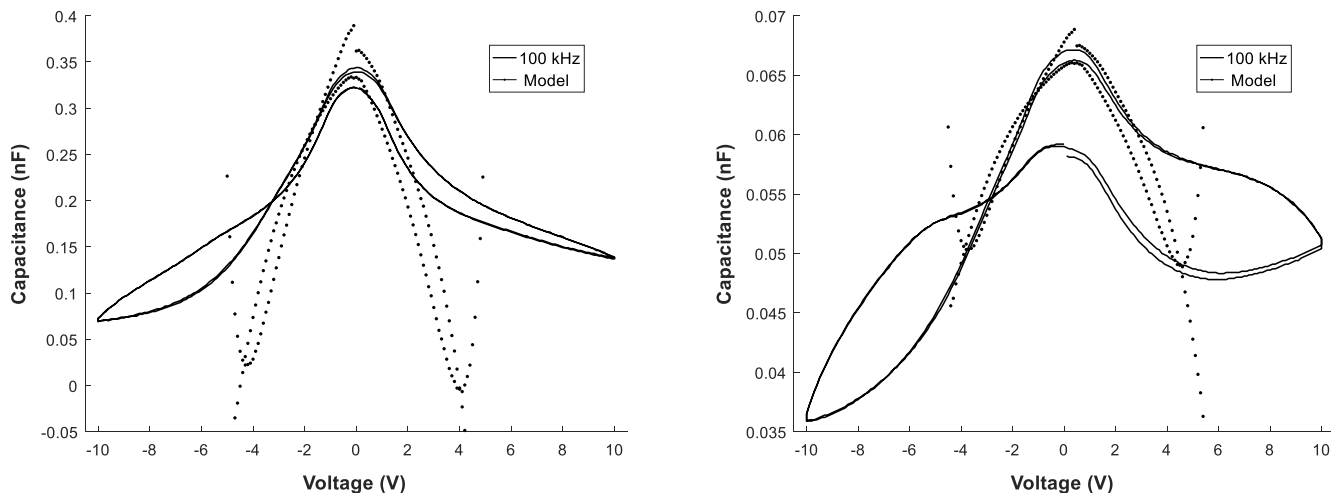
Fig. 5. Modeled diffusion capacitance C_D ($\cdot$) overlaid on $C(V)$ data measured (solid lines) at $100\,$kHz and $1\,$MHz for the Ag/UO$_2$ Schottky diode. The calculated diffusion capacitance, C_D, indicates a drift carrier lifetime in (a) of approximately $50\,\mu s$ and (b) of approximately $250\,\mu s$.

The imaginary part, ε_2, can be modeled conveniently using Gaussian functions as:

$$\varepsilon_2(E) = A\left(\exp\left(-\left(\frac{E - E_n}{\sigma}\right)^2\right)\right.$$
$$\left.-\exp\left(-\left(\frac{E + E_n}{\sigma}\right)^2\right)\right), \qquad (4)$$

$$\sigma = \frac{B_r}{2\sqrt{\ln(2)}}, \qquad (5)$$

with best-match parameters of amplitude, A, center energy, E_n, and broadening, B$_r$ [37]. The real part, ε_1, is obtained from Kramers-Kronig transformation such that:

$$\varepsilon_1(E) = \frac{2}{\pi} P \int_0^\infty \frac{\xi \varepsilon_2(\xi)}{\xi^2 - E^2} d\xi, \qquad (6)$$

where P is the principal value of the integral and ω is the angular frequency. The dielectric constants determined in this study agree very well with those presented by Siekhaus and Crowhurst [38]. However, as Siekhaus and Crowhurst discuss, there is a significant shift when compared to reflectivity measurements as determined by Schoenes [39].

While we observe a similar shape to the real and imaginary parts of the dielectric response, we find a significant shift in the critical points (CPs). Electron band-to-band transitions create CP features in a dielectric response spectra [38]. These critical points are described using Gaussian oscillators and are summarized in Table 1. A single Gaussian oscillator centered beyond the investigated spectral region at $8.02\,$eV was also used to account for high-energy contributions. A constant offset and infrared contribution were accounted for in the analysis, which are not further detailed in the table.
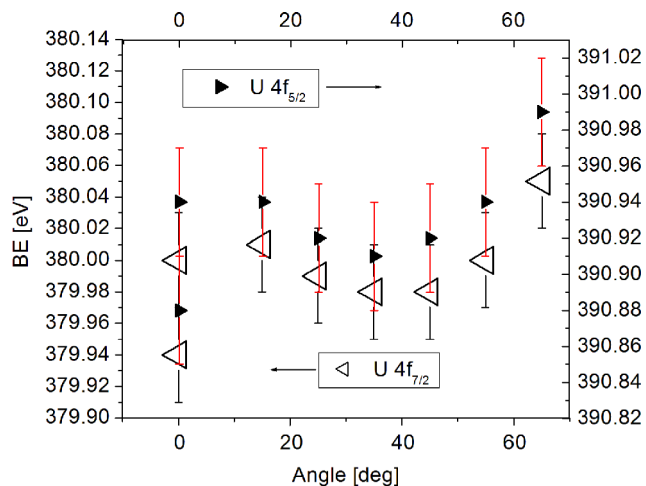
Fig. 6. The depth resolved XPS on the UO$_2$ (111). Both U $4f$ peaks shift to higher binding energies at the surface of the crystal, with increasing take off angle, indicating a chemical shift of the U to an oxidation state greater than U^{+4}.

The energetically lowest critical point was determined to have an energy of $1.99\,$eV, based on the spectral center of the absorption feature, compared to $2.4467\,$eV, as determined by Siekhaus and Crowhurst [38] also using a Gaussian oscillator absorption model. However, we cannot directly compare higher energy absorption feature values found here to those reported by Siekhaus et al., as the latter used a Tauc-Lorentz type oscillator to describe the second, higher energy, critical point with a center energy at $3.5646\,$eV and an optical gap energy of $2.7289\,$eV. The Tauc-Lorentz oscillator was developed to describe only amorphous materials [40], and while data taken from a single-crystal material may be well matched using a Tauc-Lorentz oscillator, the physical meaning behind parameters is not known. Therefore, we have estimated Gaussian parameters, as used in this work, to approximate

Table 1. Critical point transition parameters of single-crystal UO_2, obtained from spectroscopic ellipsometry data analysis of single-crystal UO_2. Parentheses denote 90% confidence of the last digit.

Feature	Critical point transitions		
	A (eV)	E (eV)	B_r (eV)
CP_1	1.5(1)	1.99(1)	1.5(1)
CP_2	3.7(5)	4.57(1)	2.4(1)
CP_3	4.6(1)	8.02(9)[1]	5.3(9)
[2]CP_1	1.8(6)	2.1(1)	1.5(2)
[2]CP_2	3(2)	3.9(1)	1.4(2)
[2]CP_3	3.3(4)	5.1(5)	3(1)

[1] Transition outside of presented range with limited sensitivity to critical point parameters.

[2] Features approximated by applying oscillators as used in this work to data gathered by Siekhaus and Crowhurst [38].
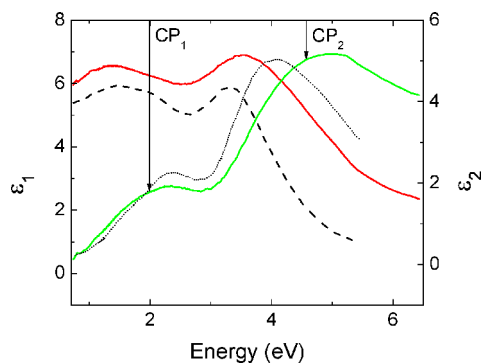
Fig. 7. Dielectric function of single-crystal UO_2 obtained in this analysis (red and green solid lines, respectively) compared to those by Siekhaus and Crowhurst [38] (black dash and dot, respectively). Both the results of Siekhaus and Crowhurst [38] and this work come from ellipsometric techniques (see text). Arrows indicating the critical points identified by our work are labeled and correspond to Gaussian oscillator parameters.

data gathered by Siekhaus et al. in order to better quantize the shift seen in Figure 7. Estimated parameters are displayed in Table 1. The energetically lowest transition is determined to be shifted by only approximately 0.1 eV, while shifts of higher transitions are more significant perhaps due to a further oxidation layer on the 25.5 year aged single-crystal UO_2 used by Siekhaus et al. [38] although this layer was not verified and it is unclear if such a layer was taken into account.

These optical transitions are feasible when considering calculated band structure, shown in Figure 1. The optical transition at roughly 2 eV is clearly connected to the band gap. The optical transitions at roughly 4.6 eV and 8 eV, corresponds to transitions from the high density of states at -2 eV and -4 eV ($E - E_F$), within the valence band, to unoccupied states at the bottom of the conduction band.

5 Conclusions

In conclusion, a metal-semiconductor Schottky barrier may be formed between the hyper-stoichiometric UO_{2+x}

and Ag, but the barrier height does not match the predicted barrier height. The C(V) measurement has a frequency dependent capacitance not normally observed in an metal-semiconductor Schottky device in reverse bias, indicating that a large defect concentration exists that may affect the ellipsometry data. A hyper-stoichiometric layer is the most likely source of this frequency dependent capacitance, which is supported by the PES data. The I(V) and $C(V)$ measurements show the bulk of the UO_2 semiconducting crystal is p-type, and makes Ohmic contacts with both E-GaIn and Ag. $C(V)$ measurements provide a drift carrier lifetime was calculated between 50–$250 \, \mu$s. This is likely due to the narrowness of the UO_{2+x} layer (<40 Å), which allows Fowler-Nordheim tunneling, and reduces the effective barrier height from 1.5 eV to 1.28 eV. Ellipsometry confirms isotropic UO_2 with an approximate 2.0 eV band gap.

In the future, any devices fabricated from UO_2 single crystals will have to account for the oxygen diffusion to interstitial sites, and take steps to suppress this, or perhaps more interestingly, make use of this layer in depositing p-type materials to form p–n heterostructures.

Author contribution statement

We state that all authors contributed to the results of this work where the revisions related to the comments of reviewers have been performed by the corresponding author Christina Dugan.

References

1. R. Stone, Science **353**, 15 (2016)
2. A. Caruso, R.B. Billa, S. Balaz, J.I. Brand, P.A. Dowben, J. Phys.: Condens. Matter **16**, L139 (2004)
3. A. Caruso, P.A. Dowben, S. Balkir, N. Schemm, K. Osberg, R.W. Fairchild, O.B. Flores, S. Balaz, A.D. Harken, B.W. Robertson, J.I. Brand, Mater. Sci. Eng. B **135**, 129 (2006)
4. N. Hong, J. Mullins, K. Foreman, S. Adenwalla, J. Phys. D: Appl. Phys. **43**, 275101 (2010)
5. G. Peterson, Q. Su, Y. Wang, P.A. Dowben, M. Nastasi, Mater. Sci. Eng. B **202**, 25 (2015)
6. E. Echeverría, B. Dong, G. Peterson, J.P. Silva, E.R. Wilson, M.S. Driver, Y.S. Jun, G.D. Stucky, S. Knight, T. Hoffman, Z.K. Han, N. Shao, Y. Gao, W.N. Mei, M. Nastasi, P.A. Dowben, J.A. Kelber, J. Appl. Phys. **49**, 355302 (2016)

7. H. Anderson, E. Fermi, L. Szilard, Phys. Rev. **56**, 284 (1939)

8. T.T. Meek, B.V. Roedern, Vacuum **83**, 226 (2008)

9. B. von Roedern, T. Meek, M. Haire, in *Symposium of the Society for the Advancement of Material and Process Engineering (SAMPE), Long Beach* (National Renewable Energy Laboratory, Golden, CO, 2003)

10. C. Kruschwitz, S. Mukhopadhyay, D. Schwellenbach, T. Meek, B. Shaver, in *Proceedings of the SPIE 9213; Hard X-Ray, Gamma-Ray, and Neutron Detector Physics XVI, San Diego* (2014)

11. C. Young, J. Petrosky, J.M. Mann, E. Hunt, D. Turner, P.A. Dowben, J. Phys.: Condens. Matter **29**, 035005-1 (2016)

12. J. Katz, E. Rabinowitch, *The chemistry of uranium* (McGraw-Hill Book Company, New York, 1951)

13. L. Lynds, W. Young, J. Mohl, G. Libowitz, *Nonstoichiometric compounds* (American Chemical Society, Washington D.C., 1963)

14. D.J. Kim, J.H. Kim, K.S. Kim, J.H. Yang, S.K. Kim, Y.H. Koo, WJNST **5**, 102 (2015)

15. B. Dorado, G. Jomard, M. Freyss, M. Bertolus, Phys. Rev. B: Condens. Matter. **82**, 035114-1 (2010)

16. T. Kelly, J. Petrosky, D. Turner, J. McClory, J. Mann, J. Kolis, X. Zhang, P. Dowben, Phys. Status Solidi RRL **8**, 283 (2014)

17. G. Leinders, T. Cardinels, K. Binnemans, M. Verwerft, J. Nucl. Mater. **459**, 135 (2015)

18. J. Holz, F.K. Schulte, H. Wagner, *Solid surface physics* (Springer, Berlin, Heidelberg, 1979)

19. R.C. Chiechi, E.A. Weiss, M.D. Dickey, G.M. Whitesides, Angew. Chem. **120**, 148 (2007)

20. G. Kresse, J. Furthmuller, Phys. Rev. B: Condens. Matter **54**, 169 (1996)

21. G. Kresse, J. Hafner, Phys. Rev. B: Condens. Matter **47**, 558 (1993)

22. G. Kresse, D. Joubert, Phys. Rev. B: Condens. Matter **59**, 1758 (1999)

23. J.P. Perdew, K. Burke, M. Ernzerhof, Phys. Rev. Lett. **77**, 3865 (1996)

24. J. Paier, M. Marsman, K. Hummer, G. Kresse, I.C. Gerber, J.G. Angyan, J. Chem. Phys. **124**, 1547091 (2006)

25. S. Dudarev, G.A. Botton, S.Y. Savarasov, C.J. Humphreys, A.P. Sutton, Phys. Rev. B **57**, 1505 (1998)

26. H. Monkhorst, J. Pack, Phys. Rev. B. **13**, 5188 (1976)

27. E. Sanville, E. Kenny, R. Smith, G. Henkelman, J. Comput. Chem. **28**, 899 (2007)

28. J. Heyd, G.S. Ernzerhob, J. Chem. Phys. **118**, 8207 (2003)

29. S. Clark, M. Segall, C. Pickard, P. Hasnip, M. Probert, K. Refson, M. Payne, Z. Kristallogr. **220**, 567 (2005)

30. S.M. Sze, K.K. Ng, *Physics of semiconductors devices*, 3rd edn. (Wiley-Interscience, New York, 2007)

31. J. Schoenes, J. Appl. Sci. **49**, 1463 (2008)

32. E. Borchi, M. Bruzzi, S. Pirollo, S. Sciortino, Solid-State Electron. **42**, 2093 (1998)

33. B.T. Willis, Acta Crystallogr. A **34**, 88 (1978)

34. I.D. Parker, J. Appl. Phys. **75**, 1656 (1994)

35. J.S. Morrell, M.J. Jackson, *Uranium processing and properties* (Springer, New York, 2013)

36. K. Gofryk, S. Du, C. Stanek, J. Lashley, X. Liu, R. Schulze, J. Smith, D. Safarik, D. Byler, K. McClellan, B. Uberuaga, B. Scott, D. Andersson, Nat. Commun. **5**, 4551 (2014)

37. A. Mock, R. Korlacki, C. Briley, D. Sekora, T. Hofmann, P. Wilson, A. Sinitskii, E. Schubert, M. Schubert, Appl. Phys. **108**, 051905-1 (2016)

38. W. Siekhaus, J. Crowhurst, IOP Conf. Ser.: Mater. Sci. Eng. **9**, 1 (2010)

39. J. Schoenes, J. Appl. Phys. **49**, 1463 (1978)

40. H. Fujiwara, *Spectroscopic ellipsometry: principles and applications* (John Wiley & Sons, West Sussex, England, 2003)